

3-[(Benzo-1,3-dioxol-5-yl)amino]-4-methoxy-cyclobut-3-ene-1,2-dione: polymorphism and twinning of a precursor to an antimycobacterial squaramide

**Paul R. Palme,^a Richard Goddard,^b Adrian Richter,^a Peter Imming^a and
Rüdiger W. Seidel^{a*}**

Received 31 May 2024
Accepted 24 June 2024

Edited by I. Oswald, University of Strathclyde,
United Kingdom

Dedicated to Professor Reinhard H. H. Neubert
on the occasion of his 75th birthday.

Keywords: squaramide; antimycobacterial agent; tuberculosis; polymorphism; twinning; hydrogen bonding; crystal structure; concomitant polymorphs.

CCDC references: 2365204; 2365205

Supporting information: this article has supporting information at journals.iucr.org/c

^aInstitut für Pharmazie, Martin-Luther-Universität Halle-Wittenberg, Wolfgang-Langenbeck-Strasse 4, 06120 Halle (Saale), Germany, and ^bMax-Planck-Institut für Kohlenforschung, Kaiser-Wilhelm-Platz 1, 45470 Mülheim an der Ruhr, Germany.

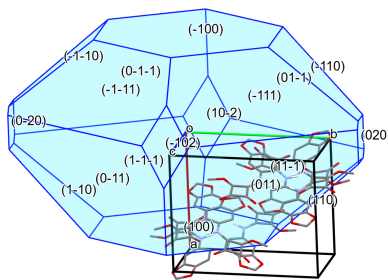
*Correspondence e-mail: ruediger.seidel@pharmazie.uni-halle.de

The title compound, 3-[(benzo-1,3-dioxol-5-yl)amino]-4-methoxycyclobut-3-ene-1,2-dione, $C_{12}H_9NO_5$ (**3**), is a precursor to an antimycobacterial squaramide. Block-shaped crystals of a monoclinic form (**3-I**, space group $P2_1/c$, $Z = 8$, $Z' = 2$) and needle-shaped crystals of a triclinic form (**3-II**, space group $P-1$, $Z = 4$, $Z' = 2$) were found to crystallize concomitantly. In both crystal forms, $R_2^2(10)$ dimers assemble through $N-H\cdots O=C$ hydrogen bonds. These dimers are formed from crystallographically unique molecules in **3-I**, but exhibit crystallographic C_i symmetry in **3-II**. Twinning by pseudomerohedry was encountered in the crystals of **3-II**. The conformations of **3** in the solid forms **3-I** and **3-II** are different from one another but are similar for the unique molecules in each polymorph. Density functional theory (DFT) calculations on the free molecule of **3** indicate that a nearly planar conformation is preferred.

1. Introduction

Mycobacterial infections constitute a substantial threat to public health globally. These can be divided into tuberculosis (TB), infections caused by nontuberculous mycobacteria (NTM; Johansen *et al.*, 2020), and leprosy (Shyam *et al.*, 2024). According to the World Health Organization (WHO), a total of 10.6 million people worldwide fell ill with TB and an estimated number of 1.1 million deaths officially classified as caused by TB was recorded in 2022 (World Health Organization, 2023). Hard-to-cure pulmonary diseases caused by NTM are also increasingly seen (Prevots *et al.*, 2023). Drug discovery efforts are vital to fill the drug development pipelines for TB and NTM disease (Dartois & Dick, 2024). In 2012, bedaquiline was the first Federal Drug Administration (FDA)-approved novel anti-TB drug since the approval of rifampicin in 1971 (Rothstein, 2016). Bedaquiline, a diarylquinolone, inhibits the proton pump of the mycobacterial ATP synthase (Andries *et al.*, 2005). Despite its success in the pharmacotherapy of multidrug-resistant TB, bedaquiline exhibits some less favourable pharmacological properties, such as QTc prolongation and drug interactions (Deshkar & Shirure, 2022). Moreover, bedaquiline-resistant strains of *Mycobacterium tuberculosis*, the etiological agent of TB, have already emerged (Khoshnood *et al.*, 2021). Therefore, the quest for new drug candidates targeting the ATP synthase in mycobacteria is pertinent.

In a target-based screening of 900 000 compounds from AstraZeneca's corporate compound collection, Tantry *et al.*



OPEN  ACCESS

Published under a CC BY 4.0 licence

(2017) discovered the compound class of squaramides as inhibitors of the mycobacterial ATP synthase. Structure–activity relationship (SAR) exploration and hit-to-lead optimization led to compound **1** with a monoamino–cyclobut-3-ene-1,2-dione scaffold [Fig. 1(a)]. Compound **1** exhibited a minimum inhibitory concentration (MIC) of 0.03 µM against the reference strain *M. tuberculosis* H37Rv *in vitro* and also showed *in vivo* efficacy in a mouse model of pulmonary TB (Tantry *et al.*, 2017). Recently, Courbon *et al.* (2023) reported the structure of **1** bound to the *Mycobacterium smegmatis* ATP synthase, as determined by cryo-electron microscopy [Fig. 1(b)]. The results show that **1** binds to a site distinct from that of bedaquiline. Through scaffold morphing and a subsequent SAR study and optimization, Li *et al.* (2020) identified the 3,4-diaminocyclobut-3-ene-1,2-dione derivative **2** [Fig. 1(c)], with a MIC of 0.45 µg ml⁻¹ (1.4 µM) against *M. tuberculosis* H37Rv. Maintaining the 2-picoly group proved important for activity and

the introduction of a benzo-1,3-dioxole group turned out to be favourable. Compound **2** was readily obtained from amidoester **3** [Fig. 1(d)] by reaction with 2-picolyamine.

In the course of our studies on antimycobacterial squaramides (Courbon *et al.*, 2023), compound **3**, the title compound, attracted our interest as a precursor to explore SARs and to optimize the potency of squaramides based on the 3,4-diaminocyclobut-3-ene-1,2-dione scaffold against *M. tuberculosis* and clinically relevant NTM species. We serendipitously discovered two concomitant polymorphs of **3**, whose crystal structures we describe in the present article. Although **3** serves only as a precursor, the observed polymorphism may have broader implications in drug development (Bhatia *et al.*, 2018). As a matter of routine, we also subjected **3** to susceptibility testing against two NTM species.

2. Experimental

2.1. General

The starting materials were purchased from BLDpharm (Shanghai, China) and used as received. Methanol was distilled before use. High-performance liquid chromatography (HPLC) analysis was conducted on a Shimadzu instrument with LC-10 AD pumps and an SPD-M10A VP PDA detector, using a Polaris 5 C18-A column (5 µm, 250 mm × 4.6 mm; Agilent Technologies, Santa Clara, CA, USA) and gradient elution with water/acetonitrile. The flow rate was 1.2 ml min⁻¹. The sample was dissolved in HPLC-grade acetonitrile prior to analysis. The NMR spectrum was recorded on an Agilent Technologies 400 MHz VNMRS spectrometer (abbreviations: *s* = singlet, *bs* = broad singlet, *d* = doublet and *bd* = broad doublet).

2.2. Synthesis and crystallization

Dimethyl squarate (1.42 g, 10 mmol) and benzo-1,3-dioxol-5-amine (1.37 g, 10 mmol) were dissolved in methanol (50 ml) and triethylamine (2.8 ml, 20 mmol) was added. The mixture was stirred overnight at room temperature. Subsequently, the precipitate was collected by centrifugation, washed with a small amount of methanol and dried in a vacuum to yield **3** as an off-white solid (yield: 2.26 g, 9.1 mmol, 91%). HPLC purity (254 nm detection): 97.5%. ¹H NMR (402 MHz, DMSO-*d*₆): δ 10.59 (*s*, 1H), 6.95 (*bs*, 1H), 6.84 (*d*, 1H), 6.75 (*bd*, 1H), 5.97 (*s*, 2H), 4.33 (*s*, 3H) ppm. Block-shaped crystals of **3-I** and needle-shaped crystals of **3-II** were found when a HPLC sample of **3** in acetonitrile had evaporated slowly to dryness under ambient conditions.

2.3. X-ray crystallography

After an initial independent atom model (IAM) refinement with *SHEXL2019* (Sheldrick, 2015b), the crystal structure of **3-I** was refined with aspherical atomic form factors using *NoSpherA2* (Kleemiss *et al.*, 2021; Midgley *et al.*, 2021) in *OLEX2* (Dolomanov *et al.*, 2009). Hirshfeld-partitioned electron density was calculated in *ORCA* (Version 5.0; Neese *et al.*, 2020) using the B3LYP method (Becke, 1993; Lee *et al.*,

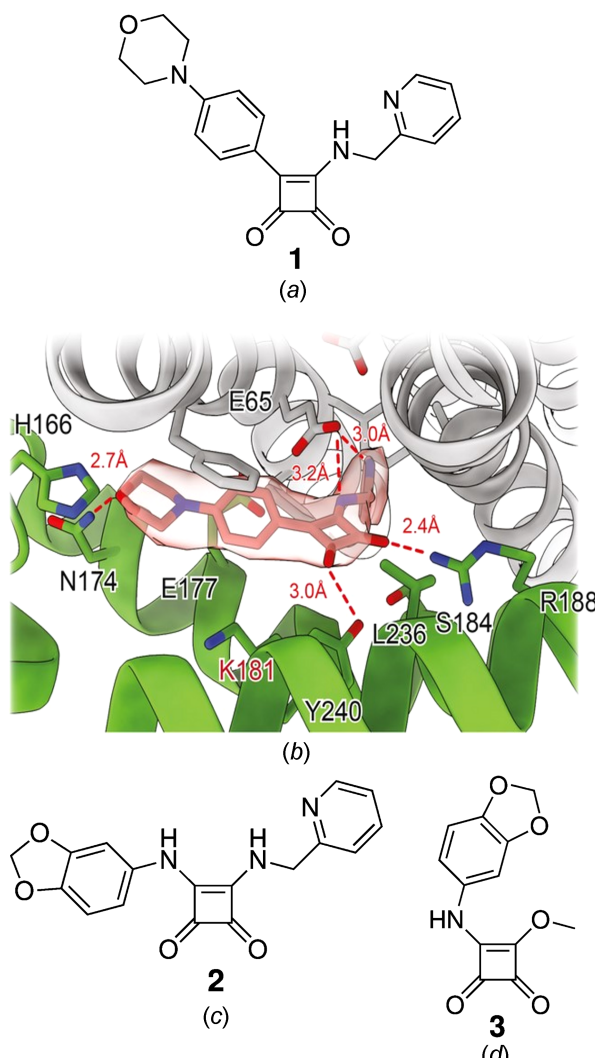


Figure 1

(a) Chemical diagram of **1** and (b) illustration of **1** in the complex with the *M. smegmatis* ATP synthase in the F₀ region (PDB entry: 8g07; Courbon *et al.*, 2023). Chemical diagrams of (c) **2** and (d) its precursor **3**, the title compound. The conformation of **3** is drawn to represent that encountered in the crystal structures reported in the present work. Part (b) was reproduced from Courbon *et al.* (2023) with permission from the publisher.

Table 1

Experimental details.

For both structures: $C_{12}H_9NO_5$. Experiments were carried out at 100 K with Mo $K\alpha$ radiation using a Bruker D8 Venture diffractometer. The absorption correction was Gaussian (*SADABS*; Bruker, 2016).

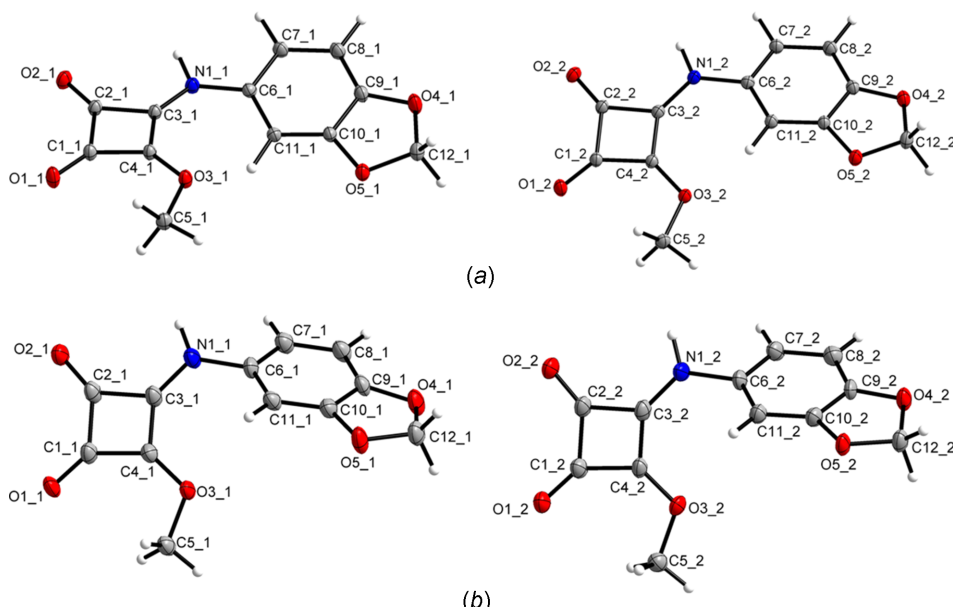
	3-I	3-II
Crystal data		
M_r	247.20	247.20
Crystal system, space group	Monoclinic, $P2_1/c$	Triclinic, $P\bar{1}$
a, b, c (Å)	13.0541 (7), 13.4304 (7), 13.1257 (7)	3.7001 (4), 12.4583 (15), 22.846 (3)
α, β, γ (°)	90, 115.354 (2), 90	89.550 (8), 86.967 (6), 81.460 (6)
V (Å ³)	2079.57 (19)	1040.0 (2)
Z	8	4
μ (mm ⁻¹)	0.13	0.13
Crystal size (mm)	0.07 × 0.07 × 0.05	0.12 × 0.05 × 0.03
Data collection		
T_{\min}, T_{\max}	0.992, 0.997	0.991, 0.998
No. of measured, independent and observed reflections	806109, 6382, 5025 [$I \geq 2\sigma(I)$]	76269, 5138, 3902 [$I > 2\sigma(I)$]
R_{int}	0.148	0.134
(sin θ/λ) _{max} (Å ⁻¹)	0.717	0.668
Refinement		
$R[F^2 > 2\sigma(F^2)], wR(F^2), S$	0.030, 0.080, 1.11	0.064, 0.170, 1.04
No. of reflections	6382	5138
No. of parameters	397	337
No. of restraints	0	1
H-atom treatment	All H-atom parameters refined	H atoms treated by a mixture of independent and constrained refinement
$\Delta\rho_{\max}, \Delta\rho_{\min}$ (e Å ⁻³)	0.24, -0.24	0.38, -0.36

Computer programs: *APEX5* (Bruker, 2022), *SAINT* (Bruker, 2019), *SHELXT* (Sheldrick, 2015a), *olex2.refine* (Bourhis *et al.*, 2015), *SHELXL* (Sheldrick, 2015b), *DIAMOND* (Brandenburg, 2018), *Mercury* (Macrae *et al.*, 2020) and *publCIF* (Westrip, 2010).

1988) and the def2-TZVPP basis set (Weigend & Ahlrichs, 2005). The positions and isotropic atomic displacement parameters were refined freely for all H atoms.

The crystal structure of **3-II** was refined using IAM refinement with *SHEXL2019*. The twinning was taken into account using TWIN and BASF instructions. Carbon-bound H atoms

were placed in geometrically calculated positions, with aromatic C—H = 0.95 Å, methylene C—H = 0.99 Å and methyl C—H = 0.98 Å, and subsequently refined using a riding model, with $U_{\text{iso}}(\text{H}) = 1.2U_{\text{eq}}(\text{C})$ (1.5 for methyl groups). The initial torsion angles of the methyl groups were determined *via* difference Fourier syntheses and subsequently refined while

**Figure 2**

The molecular structures of the crystallographically unique molecules in (a) **3-I** and (b) **3-II**. The numbers after the underscore indicate crystallographically unique molecules 1 and 2. Displacement ellipsoids are drawn at the 50% probability level. H atoms are represented by small spheres of arbitrary radius.

Table 2
Selected torsion angles ($^{\circ}$) for **3-I** and **3-II**.

	3-I	3-II
C3_1—N1_1—C6_1—C11_1	15.64	−42.0 (5)
C3_2—N1_2—C6_2—C11_2	−18.46 (11)	−49.3 (5)

maintaining a tetrahedral structure. Nitrogen-bound H atoms were located in $F_{\text{obs}} - F_{\text{calc}}$ electron-density maps and refined semi-freely. The N1—H1 distances in both crystallographically distinct molecules were restrained to be similar, with a standard uncertainty of 0.02 Å. The corresponding $U_{\text{iso}}(\text{H})$ parameters were refined freely.

BFDH (Bravais, Friedel, Donnay and Harker) morphologies (Bravais, 1866; Friedel, 1907) were calculated with *Mercury* (Macrae *et al.*, 2020), and packing indices were calculated with *PLATON* (Spek, 2020). For the latter, the H-atom positions in **3-I** and **3-II** were normalized to make the X—H distances equal to the average neutron diffraction values (C—H = 1.089 Å and N—H = 1.015 Å) (Allen & Bruno, 2010), using *Mercury*. Crystal data, data collection and structure refinement details are summarized in Table 1.

2.4. Computational methods

Density functional theory (DFT) calculations were performed using *ORCA* (Version 5.0; Neese *et al.*, 2020) with a B3LYP/G (VWN5) hybrid functional (20% HF exchange) (Becke, 1993; Lee *et al.*, 1988) using a def2-TZVPP basis set (Weigend & Ahlrichs, 2005) with an auxiliary def2/J basis (Weigend, 2006). Optimization of the structure used the BFGS method from an initial Hessian according to Almlöf's model with a very tight self-consistent field convergence threshold (Häser & Almlöf, 1992). Calculations were made on the free molecule of **3**. The input structure was taken from the crystal structure of **3-I**. The optimized local minimum-energy structure exhibited only positive modes. Cartesian coordinates of the DFT-optimized structure of **3** can be found in the supporting information.

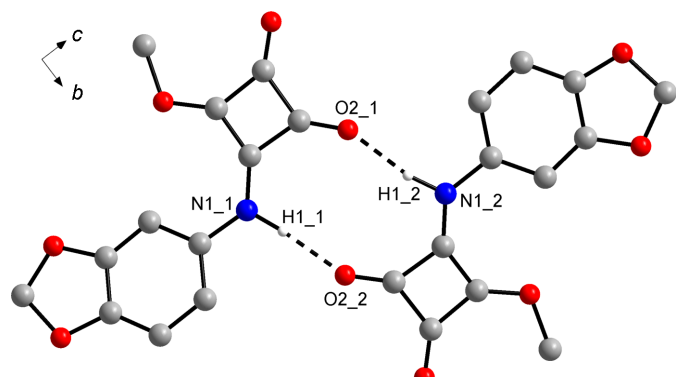


Figure 3

Hydrogen-bond dimer in the crystal structure of **3-I**. Dashed lines represent hydrogen bonds. The numbers after the underscore indicate crystallographically unique molecule 1 and 2. Carbon-bound H atoms have been omitted for clarity.

Table 3
Hydrogen-bond geometry (Å, $^{\circ}$) for **3-I**.

$D-\text{H}\cdots A$	$D-\text{H}$	$\text{H}\cdots A$	$D\cdots A$	$D-\text{H}\cdots A$
N1_1—H1_1—O2_2	1.037 (15)	1.864 (15)	2.8963 (10)	172.9 (12)
N1_2—H1_2—O2_1	1.026 (15)	1.901 (15)	2.8772 (10)	157.8 (12)

3. Results and discussion

Two polymorphic forms of **3** were found to crystallize concomitantly from a solution in acetonitrile under ambient conditions, which could be readily distinguished from one another by their external shapes. Colourless block-shaped crystals belong to a monoclinic phase (hereafter **3-I**) and colourless needle-shaped crystals correspond to a triclinic phase, in which twinning by pseudomerohedry was encountered (hereafter **3-II**).

3.1. Molecular structures of **3** in polymorphs I and II

In both polymeric forms, compound **3** crystallizes with two molecules in the asymmetric unit ($Z' = 2$). Fig. 2 depicts displacement ellipsoid plots for both crystallographically unique molecules in each crystal form. In each case, the molecules essentially exhibit the conformation shown in Fig. 1(d), albeit with some tilt between the squaramide and the benzo-1,3-dioxole moieties. In **3-I**, the angle between the mean planes through the four-membered squaramide ring and the six-membered arene ring is 13.5° for molecule 1 and 14.6° in molecule 2. The tilt is significantly larger in **3-II**, as indicated

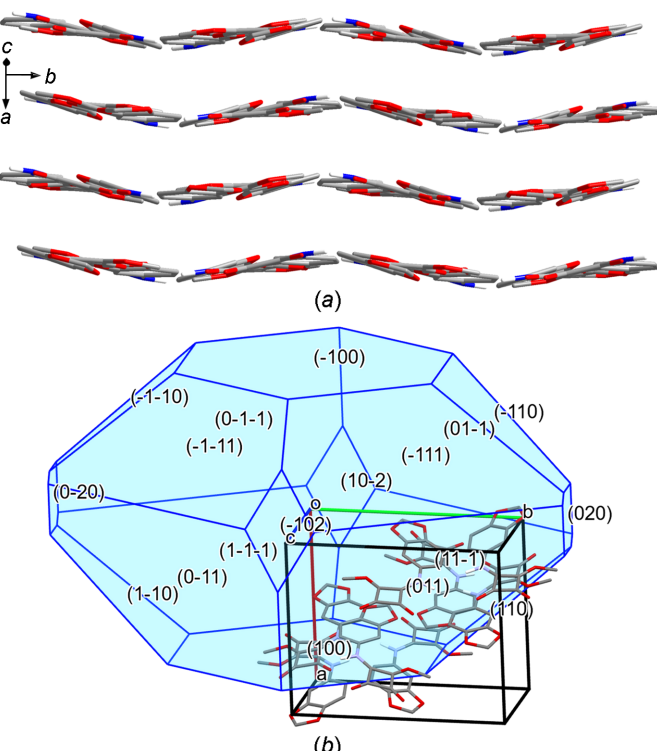


Figure 4

(a) Packing diagram of **3-I**, viewed along the [102] direction. (b) BFDH morphology calculated for **3-I**. Carbon-bound H atoms have been omitted for clarity.

Table 4Hydrogen-bond geometry (\AA , $^\circ$) for **3-II**.

$D-\text{H}\cdots A$	$D-\text{H}$	$\text{H}\cdots A$	$D\cdots A$	$D-\text{H}\cdots A$
N1_1—H1_1···O2_1 ⁱ	0.94 (3)	1.95 (4)	2.880 (4)	168 (4)
N1_2—H1_2···O2_2 ⁱⁱ	0.94 (3)	1.91 (3)	2.831 (4)	167 (4)

Symmetry codes: (i) $-x, -y + 1, -z + 1$; (ii) $-x + 1, -y, -z$.

by the angles between the aforementioned mean planes of 41.5° in molecule 1 and 49.4° in molecule 2. The C3—N1—C6—C11 torsion angles also reflect the difference in the molecular conformations in **3-I** and **3-II** (Table 2).

To evaluate the impact of the overall crystal packing on the conformation of **3**, we performed DFT calculations on the isolated molecule. The resulting minimum energy molecular structure adopts a nearly planar conformation (see supporting information), as revealed by an angle between the mean planes through the four-membered ring and the benzene ring of 5.2° and a C3—N1—C6—C11 torsion angle of -4.7° . It is worth noting that the related 3-methoxy-4-(naphthalen-2-yl-amino)cyclobut-3-ene-1,2-dione adopts approximately the same nearly planar conformation in the crystal (CSD refcode YOHROF; Avila-Costa *et al.*, 2019).

3.2. Crystal structure of the monoclinic form **3-I**

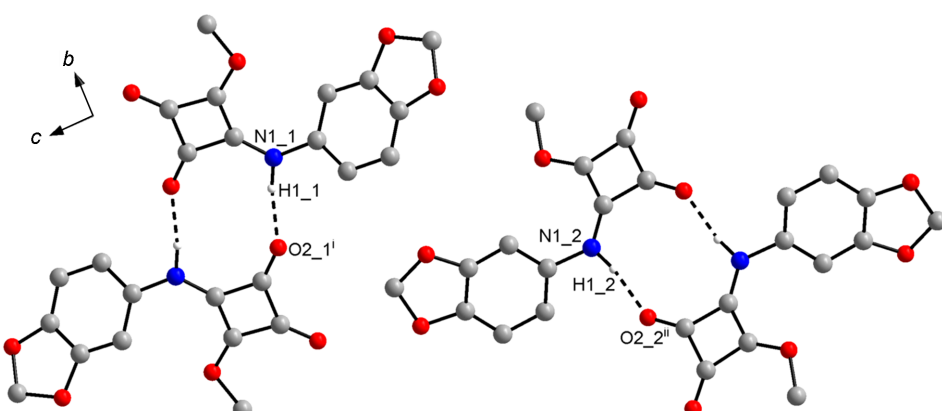
In the chosen asymmetric unit, the two crystallographically unique molecules in **3-I** form dimers through N—H···O=C hydrogen bonds between the amide group and the carbonyl group of an adjacent molecule (Fig. 3), similar to the above-mentioned YOHROF. The graph-set descriptor is $R_2^2(10)$ (Bernstein *et al.*, 1995). Table 3 lists the corresponding hydrogen-bond parameters. Although the hydrogen-bond dimers so formed lack crystallographic symmetry and their structure also markedly deviates from approximate local C_i symmetry, it is interesting to note that the two unique molecules that form a dimer represent enantiomeric conformers, as indicated by the signs of the C3—N1—C6—C11 torsion angles (Table 2). The crystal packing in **3-I** is remarkably

dense, as revealed by a calculated packing index of 76.4% (Kitajgorodskij, 1973) and the calculated crystal density (Table 1). The hydrogen-bond dimers form stacks to give corrugated sheets in the crystal, as revealed by a view along the [102] direction [Fig. 4(a)]. The most prominent feature is stacking of the arene ring of unique molecule 1 and the squaramide ester moiety of unique molecule 2 in adjacent sheets. The distance between the corresponding ring centroids is 3.31 \AA . The BFDH morphology calculation, as shown in Fig. 4(b), predicts the shape of the crystals (see supporting information) roughly correctly.

3.3. Crystal structure of the triclinic form **3-II**

The crystal structure of the triclinic polymorph **3-II** likewise features dimers formed through N—H···O=C hydrogen bonds with an $R_2^2(10)$ motif (Fig. 5). Table 4 lists the associated hydrogen-bond parameters. In contrast to **3-I**, the hydrogen-bond dimers are not formed by crystallographically distinct molecules, but each of the two unique molecules forms a dimer about a crystallographic inversion centre with a symmetry-related molecule (Fig. 5). The calculated crystallographic density of **3-II** is virtually equal to that of the monoclinic phase **3-I** (Table 1). Likewise, the packing index calculated for **3-II** at 76.7% is nearly the same as that of **3-I**. In contrast to **3-I**, the arene rings and the squaramide moieties of adjacent molecules each assemble to form stacks. The distances between the ring mean planes are *ca* 3.3 \AA . The centroid–centroid separation is 3.70 \AA in each case (corresponding to the a lattice parameter). The overall crystal packing of **3-II** is distinctly different from that of **3-I**. As shown in Fig. 6(a), a view along the [201] direction reveals a herringbone-like pattern. As for **3-I**, the BFDH morphology calculation predicts the needle shape of the crystals of **3-II** roughly correctly, with the a axis representing the needle axis [Fig. 6(b)].

The crystals of **3-II** were twinned by pseudomerohedry (Parkin, 2021; Parsons, 2003). The conventional triclinic primitive cell of **3-II** can be transformed to a C -centred cell as follows:

**Figure 5**

Hydrogen-bond dimers in the crystal structure of **3-II**. Dashed lines represent hydrogen bonds. The numbers after the underscore indicate crystallographically unique molecules 1 and 2. Carbon-bound H atoms have been omitted for clarity. [Symmetry codes: (i) $-x, -y + 1, -z + 1$; (ii) $-x + 1, -y, -z$.]

$$\begin{pmatrix} \mathbf{a}' \\ \mathbf{b}' \\ \mathbf{c}' \end{pmatrix} = \begin{pmatrix} -1 & 0 & 0 \\ 1 & -2 & 0 \\ 0 & 0 & 1 \end{pmatrix} \begin{pmatrix} \mathbf{a} \\ \mathbf{b} \\ \mathbf{c} \end{pmatrix}$$

The *C*-centred cell so obtained simulates monoclinic metrics with $a' = 3.700$, $b' = 24.640$, $c' = 22.846$ Å and $\beta' = 93.03^\circ$. The twin operation in the nonstandard space group setting $C\bar{1}$ is a twofold rotation about the *b*-axis direction:

$$2_{[010]} = \begin{pmatrix} -1 & 0 & 0 \\ 0 & 1 & 0 \\ 0 & 0 & -1 \end{pmatrix}$$

A mirror operation about the plane perpendicular to the *b*-axis direction of the *C*-centred cell is an equal description of the twinning. The second twin component relative to the reduced cell can be derived from:

$$\begin{pmatrix} -1 & 0 & 0 \\ 0 & 1 & 0 \\ 0 & 0 & -1 \end{pmatrix} \begin{pmatrix} -1 & 0 & 0 \\ 1 & -2 & 0 \\ 0 & 0 & 1 \end{pmatrix} = \begin{pmatrix} 1 & 0 & 0 \\ 1 & -2 & 0 \\ 0 & 0 & -1 \end{pmatrix}$$

The twin operation expressed with respect to the reduced cell can then be calculated as follows:

$$\begin{pmatrix} -1 & 0 & 0 \\ 1 & -2 & 0 \\ 0 & 0 & 1 \end{pmatrix}^{-1} \begin{pmatrix} 1 & 0 & 0 \\ 1 & -2 & 0 \\ 0 & 0 & -1 \end{pmatrix} = \begin{pmatrix} -1 & 0 & 0 \\ -1 & 1 & 0 \\ 0 & 0 & -1 \end{pmatrix}$$

In the triclinic axis system of the reduced cell, this represents a twofold rotation about the $[\bar{1}20]$ direction. Fig. 7 shows the relationship between the pseudo-monoclinic *C*-centred unit cell and the two twin components with respect to the primitive triclinic cell. The ratio of the fractional volume contributions of the two twin components refined to 0.584 (2): 0.416 (2). A similar case of twinning by pseudomeroedry of a triclinic crystal of an organic compound was reported by Bolte & Kettner (1998).

3.4. Antimycobacterial evaluation

We wondered whether compound **3** as a precursor to antimycobacterial squaramides (Li *et al.*, 2020) might itself exhibit antimycobacterial activity. Therefore, we evaluated its activity against the NTM species *Mycobacterium smegmatis* and *Mycobacterium abscessus* subsp. *abscessus*. *M. smegmatis* is a generally considered non-pathogenic model organism in early-stage anti-TB drug discovery (Sundarsingh *et al.*, 2020), whereas *M. abscessus* is an opportunistic pathogen, which can cause difficult-to-treat lung disease resembling pulmonary TB and extrapulmonary infections in susceptible hosts (Abdelaal *et al.*, 2022). We performed susceptibility testing against *M. smegmatis* mc² 155 pTEC27 and *M. abscessus* ATCC 19977 pTEC27 (expressing tomato red fluorescent protein) using the broth microdilution method (Middlebrook 7H9 medium supplemented with 10% albumin–dextrose–saline and containing 0.05% polysorbate 80) with optical density and fluorescence based readout, as described previously (Lang *et al.*, 2023). Up to a compound concentration of 100 µM, however, no growth inhibition of the two aforementioned mycobacterial strains was observed. The results appear to be in line with the SAR

studies reported by Tantry *et al.* (2017) and Li *et al.* (2020), which found that the 2-picoly group is critical for activity against *M. tuberculosis* H37Rv.

4. Conclusions

We report two concomitant polymorphs of the title compound **3** and structurally characterized them by X-ray crystallography. Both the monoclinic form **3-I** and the triclinic form **3-II** were found to crystallize with two molecules in the asymmetric unit ($Z' = 2$). The molecular conformations differ significantly between the two polymorphs and variously differ depending on the polymorph. DFT calculations on the isolated molecule suggest that a planar conformation is preferred. Whereas the

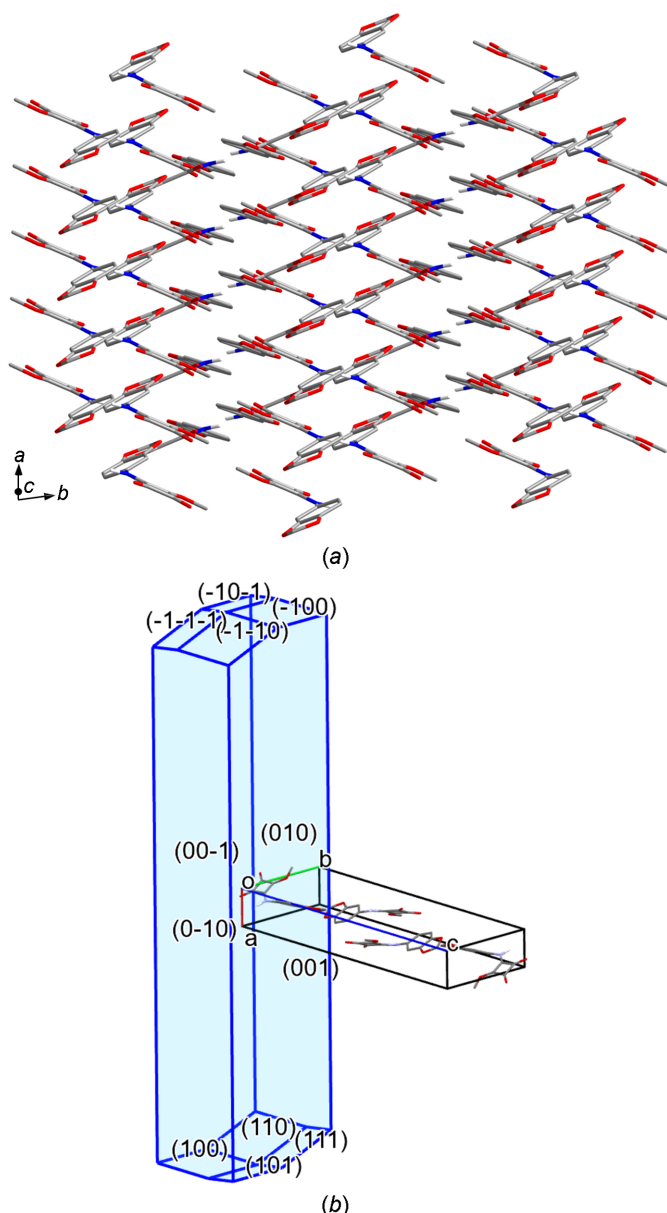
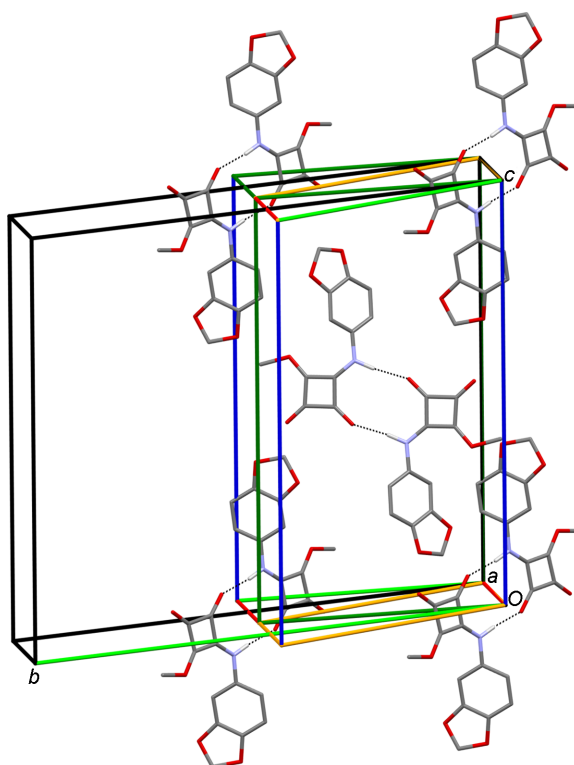


Figure 6

(a) Packing diagram of **3-II**, viewed along the $[20\bar{1}]$ direction. (b) BFDH morphology calculated for **3-II**. Carbon-bound H atoms have been omitted for clarity.

**Figure 7**

Part of the crystal structure of **3-II** (molecules in the major twin component) and the relationship between the pseudo-monoclinic *C*-centred unit cell (black line) and the two twin components with respect to the triclinic primitive cell (dark-green and orange lines). Dashed lines represent hydrogen bonds. Carbon-bound H atoms have been omitted for clarity.

packing of the molecules in **3-I** is characterized by alternate stacking of arene rings and squaramide ester moieties of adjacent molecules, in **3-II**, these groups each assemble to form columns. Crystallographic densities and packing indices calculated for **3-I** and **3-II** indicate that the crystal packing is equally dense within experimental error, which suggests that the difference in energy between the two polymorphs is small. This possibly explains why concomitant crystallization of both crystal forms occurred. As expected, and consistent with previous SAR studies, no *in vitro* activity of **3** against two mycobacterial strains was observed.

Acknowledgements

We would like to thank Professor Christian W. Lehmann for providing access to the X-ray diffraction facility, Heike Schucht and Lucas Schulte-Zweckel for technical assistance with the X-ray intensity data collections, and Dr Jens-Ulrich Rahfeld, Dr Nadine Taudte and Nadine Jänckel for providing and maintaining the biosafety level 2 laboratory. Open access funding enabled and organized by Projekt DEAL.

Funding information

Funding for this research was provided by: German Research Foundation (DFG) (grant No. 432291016 to Adrian Richter);

Mukoviszidose Institut gGmbH (Bonn, Germany), the research and development arm of the German Cystic Fibrosis Association Mukoviszidose e.V. (grant No. 2202 to Adrian Richter).

References

- Abdelal, H. F. M., Chan, E. D., Young, L., Baldwin, S. L. & Coler, R. N. (2022). *Microorganisms*, **10**, 1454.
- Allen, F. H. & Bruno, I. J. (2010). *Acta Cryst. B* **66**, 380–386.
- Andries, K., Verhasselt, P., Guillemont, J., Göhlmann, H. W. H., Neefs, J.-M., Winkler, H., Van Gestel, J., Timmerman, P., Zhu, M., Lee, E., Williams, P., de Chaffoy, D., Huitric, E., Hoffner, S., Cambau, E., Truffot-Pernot, C., Lounis, N. & Jarlier, V. (2005). *Science*, **307**, 223–227.
- Ávila-Costa, M., Donnici, C. L., dos Santos, J. D., Diniz, R., Barros-Barbosa, A., Cuin, A. & de Oliveira, L. F. C. (2019). *Spectrochim. Acta A Mol. Biomol. Spectrosc.* **223**, 117354.
- Becke, A. D. (1993). *J. Chem. Phys.* **98**, 5648–5652.
- Bernstein, J., Davis, R. E., Shimoni, L. & Chang, N.-L. (1995). *Angew. Chem. Int. Ed. Engl.* **34**, 1555–1573.
- Bhatia, A., Chopra, S., Nagpal, K., Deb, P. K., Tekade, M. & Tekade, R. K. (2018). *Polymorphism and its Implications in Pharmaceutical Product Development*, ch. 2, in *Advances in Pharmaceutical Product Development and Research, Dosage Form Design Parameters*, edited by R. K. Tekade, pp. 31–65. London: Academic Press.
- Bolte, M. & Kettner, M. (1998). *Acta Cryst. C* **54**, 963–964.
- Bourhis, L. J., Dolomanov, O. V., Gildea, R. J., Howard, J. A. K. & Puschmann, H. (2015). *Acta Cryst. A* **71**, 59–75.
- Brandenburg, K. (2018). DIAMOND. Crystal Impact GbR, Bonn, Germany.
- Bravais, A. (1866). *Etudes Cristallographiques*. Paris: Gauthier-Villars.
- Bruker (2016). SADABS. Bruker AXS Inc., Madison, Wisconsin, USA.
- Bruker (2019). SAINT. Bruker AXS Inc., Madison, Wisconsin, USA.
- Bruker (2022). APEX5. Bruker AXS Inc., Madison, Wisconsin, USA.
- Courbon, G. M., Palme, P. R., Mann, L., Richter, A., Imming, P. & Rubinstein, J. L. (2023). *EMBO J.* **42**, e113687.
- Dartois, V. & Dick, T. (2024). *Nat. Rev. Drug Discov.* **23**, 381–403.
- Deshkar, A. T. & Shirure, P. A. (2022). *Cureus*, **14**, e28519.
- Dolomanov, O. V., Bourhis, L. J., Gildea, R. J., Howard, J. A. K. & Puschmann, H. (2009). *J. Appl. Cryst.* **42**, 339–341.
- Friedel, G. (1907). *Bull. Soc. Fr. Miner.* **30**, 326–455.
- Häser, M. & Almlöf, J. (1992). *J. Chem. Phys.* **96**, 489–494.
- Johansen, M. D., Herrmann, J. L. & Kremer, L. (2020). *Nat. Rev. Microbiol.* **18**, 392–407.
- Khoshnood, S., Goudarzi, M., Taki, E., Darbandi, A., Kouhsari, E., Heidary, M., Motahar, M., Moradi, M. & Bazyar, H. (2021). *J. Glob. Antimicrob. Resist.* **25**, 48–59.
- Kitajgorodskij, A. I. (1973). In *Molecular Crystals and Molecules*. London: Academic Press.
- Kleemiss, F., Dolomanov, O. V., Bodensteiner, M., Peyerimhoff, N., Midgley, M., Bourhis, L. J., Genoni, A., Malaspina, L. A., Jayatlaka, D., Spencer, J. L., White, F., Grundköetter-Stock, B., Steinhauer, S., Lentz, D., Puschmann, H. & Grabowsky, S. (2021). *Chem. Sci.* **12**, 1675–1692.
- Lang, M., Ganapathy, U. S., Mann, L., Abdelaziz, R., Seidel, R. W., Goddard, R., Sequenzia, I., Hoenke, S., Schulze, P., Aragaw, W. W., Csuk, R., Dick, T. & Richter, A. (2023). *J. Med. Chem.* **66**, 5079–5098.
- Lee, C., Yang, W. & Parr, R. G. (1988). *Phys. Rev. B* **37**, 785–789.
- Li, P., Wang, B., Li, G., Fu, L., Zhang, D., Lin, Z., Huang, H. & Lu, Y. (2020). *Eur. J. Med. Chem.* **206**, 112538.

- Macrae, C. F., Sovago, I., Cottrell, S. J., Galek, P. T. A., McCabe, P., Pidcock, E., Platings, M., Shields, G. P., Stevens, J. S., Towler, M. & Wood, P. A. (2020). *J. Appl. Cryst.* **53**, 226–235.
- Midgley, L., Bourhis, L. J., Dolomanov, O. V., Grabowsky, S., Kleemiss, F., Puschmann, H. & Peyerimhoff, N. (2021). *Acta Cryst. A* **77**, 519–533.
- Neese, F., Wennmohs, F., Becker, U. & Riplinger, C. (2020). *J. Chem. Phys.* **152**, 224108.
- Parkin, S. R. (2021). *Acta Cryst. E* **77**, 452–465.
- Parsons, S. (2003). *Acta Cryst. D* **59**, 1995–2003.
- Prevots, D. R., Marshall, J. E., Wagner, D. & Morimoto, K. (2023). *Clin. Chest Med.* **44**, 675–721.
- Rothstein, D. M. (2016). *Cold Spring Harb. Perspect. Med.* **6**, a027011.
- Sheldrick, G. M. (2015a). *Acta Cryst. A* **71**, 3–8.
- Sheldrick, G. M. (2015b). *Acta Cryst. C* **71**, 3–8.
- Shyam, M., Kumar, S. & Singh, V. (2024). *Infect. Dis.* **10**, 251–269.
- Spek, A. L. (2020). *Acta Cryst. E* **76**, 1–11.
- Sundarsingh, J. A. T., Ranjitha, J., Rajan, A. & Shankar, V. (2020). *J. Infect. Public Health*, **13**, 1255–1264.
- Tantry, S. J., Markad, S. D., Shinde, V., Bhat, J., Balakrishnan, G., Gupta, A. K., Ambady, A., Raichurkar, A., Kedari, C., Sharma, S., Mudugal, N. V., Narayan, A., Naveen Kumar, C. N., Nanduri, R., Bharath, S., Reddy, J., Panduga, V., Prabhakar, K. R., Kandaswamy, K., Saralaya, R., Kaur, P., Dinesh, N., Guptha, S., Rich, K., Murray, D., Plant, H., Preston, M., Ashton, H., Plant, D., Walsh, J., Alcock, P., Naylor, K., Collier, M., Whiteaker, J., McLaughlin, R. E., Mallya, M., Panda, M., Rudrapatna, S., Ramachandran, V., Shandil, R., Sambandamurthy, V. K., Mdluli, K., Cooper, C. B., Rubin, H., Yano, T., Iyer, P., Narayanan, S., Kavanagh, S., Mukherjee, K., Balasubramanian, V., Hosagrahara, V. P., Solapure, S., Ravishankar, S. & Hameed, P. S. (2017). *J. Med. Chem.* **60**, 1379–1399.
- Weigend, F. (2006). *Phys. Chem. Chem. Phys.* **8**, 1057–1065.
- Weigend, F. & Ahlrichs, R. (2005). *Phys. Chem. Chem. Phys.* **7**, 3297–3305.
- Westrip, S. P. (2010). *J. Appl. Cryst.* **43**, 920–925.
- World Health Organization (2023). *Global Tuberculosis Report 2023*. Geneva: World Health Organization.

supporting information

Acta Cryst. (2024). C80 [https://doi.org/10.1107/S2053229624006211]

3-[(Benzo-1,3-dioxol-5-yl)amino]-4-methoxycyclobut-3-ene-1,2-dione: polymorphism and twinning of a precursor to an antimycobacterial squaramide

Paul R. Palme, Richard Goddard, Adrian Richter, Peter Imming and Rüdiger W. Seidel

Computing details

3-[(Benzo-1,3-dioxol-5-yl)amino]-4-methoxycyclobut-3-ene-1,2-dione (3-I)

Crystal data

$C_{12}H_9NO_5$	$F(000) = 1024.847$
$M_r = 247.21$	$D_x = 1.579 \text{ Mg m}^{-3}$
Monoclinic, $P2_1/c$	Mo $K\alpha$ radiation, $\lambda = 0.71073 \text{ \AA}$
$a = 13.0541 (7) \text{ \AA}$	Cell parameters from 9631 reflections
$b = 13.4304 (7) \text{ \AA}$	$\theta = 2.3\text{--}25.0^\circ$
$c = 13.1257 (7) \text{ \AA}$	$\mu = 0.13 \text{ mm}^{-1}$
$\beta = 115.354 (2)^\circ$	$T = 100 \text{ K}$
$V = 2079.57 (19) \text{ \AA}^3$	Block, colourless
$Z = 8$	$0.07 \times 0.07 \times 0.05 \text{ mm}$

Data collection

Bruker D8 Venture diffractometer	806109 measured reflections 6382 independent reflections 5025 reflections with $I \geq 2\sigma(I)$
Radiation source: I μ S-Diamond	$R_{\text{int}} = 0.148$
Montel multilayer optics monochromator	$\theta_{\max} = 30.7^\circ, \theta_{\min} = 2.3^\circ$
Detector resolution: 7.391 pixels mm^{-1}	$h = -18 \rightarrow 18$
φ - and ω -scans	$k = -19 \rightarrow 19$
Absorption correction: gaussian (SADABS; Bruker, 2016)	$l = -18 \rightarrow 18$
$T_{\min} = 0.992, T_{\max} = 0.997$	

Refinement

Refinement on F^2	Secondary atom site location: difference Fourier map
Least-squares matrix: full	Hydrogen site location: difference Fourier map
$R[F^2 > 2\sigma(F^2)] = 0.030$	All H-atom parameters refined
$wR(F^2) = 0.080$	$w = 1/[\sigma^2(F_o^2) + (0.0302P)^2 + 0.5221P]$ where $P = (F_o^2 + 2F_c^2)/3$
$S = 1.11$	$(\Delta/\sigma)_{\max} = -0.0002$
6382 reflections	$\Delta\rho_{\max} = 0.24 \text{ e \AA}^{-3}$
397 parameters	$\Delta\rho_{\min} = -0.24 \text{ e \AA}^{-3}$
0 restraints	
0 constraints	
Primary atom site location: dual	

Special details

Experimental. Crystal mounted on a MiTeGen loop using Perfluoropolyether Fomblin YR-1800

Refinement. Refinement using NoSpherA2, an implementation of NOn-SPHERical Atom-form-factors in Olex2. Please cite: F. Kleemiss *et al.* Chem. Sci. DOI 10.1039/D0SC05526C - 2021 NoSpherA2 implementation of HAR makes use of tailor-made aspherical atomic form factors calculated on-the-fly from a Hirshfeld-partitioned electron density (ED) - not from spherical-atom form factors.

The ED is calculated from a gaussian basis set single determinant SCF wavefunction - either Hartree-Fock or DFT using selected functionals - for a fragment of the crystal. This fragment can be embedded in an electrostatic crystal field by employing cluster charges or modelled using implicit solvation models, depending on the software used. The following options were used: SOFTWARE: ORCA 5.0 PARTITIONING: NoSpherA2 INT ACCURACY: Normal METHOD: B3LYP BASIS SET: def2-TZVPP CHARGE: 0 MULTIPLICITY: 1 DATE: 2024-02-18_15-57-08

Fractional atomic coordinates and isotropic or equivalent isotropic displacement parameters (\AA^2)

	<i>x</i>	<i>y</i>	<i>z</i>	$U_{\text{iso}}^*/U_{\text{eq}}$
C1_1	0.26369 (8)	0.44697 (7)	0.27179 (7)	0.01613 (17)
C2_1	0.27221 (7)	0.55888 (7)	0.26774 (7)	0.01554 (16)
C3_1	0.21158 (7)	0.55434 (7)	0.14363 (7)	0.01429 (16)
C4_1	0.20786 (7)	0.44933 (7)	0.14776 (7)	0.01447 (16)
C5_1	0.17077 (9)	0.27915 (7)	0.10794 (8)	0.01873 (18)
H5A_1	0.1246 (12)	0.2748 (10)	0.1589 (11)	0.042 (4)*
H5B_1	0.1331 (13)	0.2336 (11)	0.0338 (13)	0.052 (4)*
H5C_1	0.2576 (11)	0.2572 (10)	0.1573 (11)	0.039 (3)*
C6_1	0.11785 (7)	0.62620 (7)	-0.04802 (7)	0.01495 (16)
C7_1	0.11598 (8)	0.71211 (7)	-0.10882 (8)	0.01770 (18)
H7_1	0.1592 (11)	0.7776 (10)	-0.0630 (10)	0.031 (3)*
C8_1	0.05948 (8)	0.71394 (7)	-0.22702 (8)	0.01946 (18)
H8_1	0.0582 (12)	0.7803 (10)	-0.2737 (11)	0.040 (4)*
C9_1	0.00739 (8)	0.62721 (7)	-0.28028 (8)	0.01795 (18)
C10_1	0.00833 (7)	0.54273 (7)	-0.21896 (7)	0.01528 (16)
C11_1	0.06101 (7)	0.53926 (7)	-0.10312 (7)	0.01539 (17)
H11_1	0.0572 (11)	0.4714 (10)	-0.0596 (11)	0.032 (3)*
C12_1	-0.08091 (9)	0.50525 (8)	-0.40248 (8)	0.02020 (19)
H12A_1	-0.1725 (12)	0.4984 (10)	-0.4494 (11)	0.040 (3)*
H12B_1	-0.0339 (11)	0.4646 (10)	-0.4388 (11)	0.041 (3)*
N1_1	0.17809 (7)	0.62977 (6)	0.07064 (6)	0.01611 (15)
H1_1	0.2063 (12)	0.7000 (11)	0.1037 (12)	0.029 (3)*
O1_1	0.28910 (7)	0.38475 (5)	0.34562 (6)	0.02350 (15)
O2_1	0.31200 (6)	0.62523 (5)	0.33642 (6)	0.02118 (15)
O3_1	0.16809 (6)	0.38102 (5)	0.06912 (5)	0.01823 (14)
O4_1	-0.05020 (7)	0.60814 (6)	-0.39294 (6)	0.02496 (16)
O5_1	-0.05040 (6)	0.46787 (5)	-0.29030 (5)	0.01980 (14)
C1_2	0.23258 (8)	1.00458 (7)	0.22341 (7)	0.01576 (17)
C2_2	0.26011 (8)	0.89563 (7)	0.22196 (7)	0.01526 (16)
C3_2	0.32099 (7)	0.89865 (7)	0.34671 (7)	0.01437 (16)
C4_2	0.29175 (7)	0.99967 (7)	0.34681 (7)	0.01422 (16)
C5_2	0.27582 (9)	1.16532 (7)	0.39345 (8)	0.01903 (18)
H5A_2	0.1836 (12)	1.1683 (10)	0.3457 (12)	0.045 (4)*
H5B_2	0.3033 (11)	1.2105 (10)	0.4681 (11)	0.042 (4)*

H5C_2	0.3154 (12)	1.1910 (10)	0.3415 (12)	0.042 (4)*
C6_2	0.42635 (8)	0.82361 (7)	0.53578 (7)	0.01480 (17)
C7_2	0.44992 (8)	0.73029 (7)	0.58741 (8)	0.01704 (17)
H7_2	0.4288 (11)	0.6627 (10)	0.5361 (11)	0.036 (3)*
C8_2	0.49833 (8)	0.72046 (7)	0.70496 (8)	0.01809 (18)
H8_2	0.5161 (12)	0.6466 (11)	0.7449 (12)	0.042 (4)*
C9_2	0.52104 (8)	0.80678 (7)	0.76698 (7)	0.01549 (17)
C10_2	0.49879 (7)	0.89956 (7)	0.71534 (7)	0.01472 (16)
C11_2	0.45216 (8)	0.91158 (7)	0.60026 (7)	0.01543 (17)
H11_2	0.4357 (11)	0.9850 (10)	0.5620 (11)	0.032 (3)*
C12_2	0.58083 (9)	0.92240 (7)	0.90227 (8)	0.01991 (19)
H12A_2	0.5420 (11)	0.9458 (10)	0.9575 (11)	0.042 (4)*
H12B_2	0.6707 (12)	0.9374 (11)	0.9375 (12)	0.047 (4)*
N1_2	0.37637 (7)	0.82530 (6)	0.41670 (6)	0.01615 (15)
H1_2	0.3660 (12)	0.7574 (11)	0.3778 (12)	0.031 (3)*
O1_2	0.18218 (6)	1.06711 (5)	0.15251 (6)	0.02236 (15)
O2_2	0.23957 (6)	0.83191 (5)	0.15024 (6)	0.01967 (14)
O3_2	0.30968 (6)	1.06339 (5)	0.42876 (5)	0.01656 (13)
O4_2	0.56380 (6)	0.81791 (5)	0.88150 (6)	0.02041 (14)
O5_2	0.52757 (6)	0.97254 (5)	0.79554 (5)	0.02011 (14)

Atomic displacement parameters (\AA^2)

	U^{11}	U^{22}	U^{33}	U^{12}	U^{13}	U^{23}
C1_1	0.0198 (4)	0.0155 (4)	0.0117 (4)	0.0002 (3)	0.0053 (3)	-0.0004 (3)
C2_1	0.0176 (4)	0.0143 (4)	0.0131 (4)	-0.0009 (3)	0.0050 (3)	-0.0021 (3)
C3_1	0.0160 (4)	0.0139 (4)	0.0119 (4)	-0.0005 (3)	0.0050 (3)	-0.0013 (3)
C4_1	0.0176 (4)	0.0135 (4)	0.0114 (4)	0.0003 (3)	0.0054 (3)	-0.0007 (3)
C5_1	0.0232 (5)	0.0148 (4)	0.0167 (4)	0.0000 (3)	0.0072 (4)	-0.0005 (3)
C6_1	0.0167 (4)	0.0149 (4)	0.0137 (4)	0.0000 (3)	0.0070 (3)	0.0004 (3)
C7_1	0.0211 (4)	0.0149 (4)	0.0160 (4)	-0.0006 (3)	0.0069 (3)	0.0014 (3)
C8_1	0.0243 (5)	0.0170 (4)	0.0165 (4)	0.0003 (4)	0.0081 (4)	0.0034 (3)
C9_1	0.0212 (4)	0.0180 (4)	0.0137 (4)	0.0011 (3)	0.0065 (3)	0.0030 (3)
C10_1	0.0169 (4)	0.0165 (4)	0.0121 (4)	0.0005 (3)	0.0059 (3)	0.0016 (3)
C11_1	0.0169 (4)	0.0154 (4)	0.0134 (4)	-0.0012 (3)	0.0060 (3)	0.0006 (3)
C12_1	0.0213 (5)	0.0239 (5)	0.0134 (4)	-0.0001 (4)	0.0056 (4)	0.0006 (3)
N1_1	0.0193 (4)	0.0139 (3)	0.0136 (3)	-0.0005 (3)	0.0057 (3)	-0.0005 (3)
O1_1	0.0345 (4)	0.0178 (3)	0.0132 (3)	0.0020 (3)	0.0055 (3)	0.0019 (3)
O2_1	0.0264 (3)	0.0179 (3)	0.0156 (3)	-0.0031 (3)	0.0054 (3)	-0.0039 (3)
O3_1	0.0253 (3)	0.0149 (3)	0.0123 (3)	0.0002 (3)	0.0061 (3)	-0.0010 (2)
O4_1	0.0342 (4)	0.0229 (4)	0.0137 (3)	-0.0013 (3)	0.0065 (3)	0.0036 (3)
O5_1	0.0246 (3)	0.0189 (3)	0.0134 (3)	-0.0026 (3)	0.0058 (3)	-0.0002 (2)
C1_2	0.0195 (4)	0.0144 (4)	0.0122 (4)	-0.0001 (3)	0.0056 (3)	0.0002 (3)
C2_2	0.0185 (4)	0.0144 (4)	0.0128 (4)	-0.0004 (3)	0.0066 (3)	-0.0012 (3)
C3_2	0.0160 (4)	0.0145 (4)	0.0126 (4)	0.0000 (3)	0.0060 (3)	-0.0010 (3)
C4_2	0.0166 (4)	0.0135 (4)	0.0125 (4)	-0.0007 (3)	0.0062 (3)	-0.0006 (3)
C5_2	0.0251 (5)	0.0149 (4)	0.0172 (4)	0.0008 (3)	0.0091 (4)	-0.0009 (3)
C6_2	0.0166 (4)	0.0143 (4)	0.0132 (4)	0.0006 (3)	0.0061 (3)	0.0000 (3)

C7_2	0.0209 (4)	0.0136 (4)	0.0152 (4)	0.0002 (3)	0.0065 (3)	-0.0001 (3)
C8_2	0.0228 (4)	0.0147 (4)	0.0158 (4)	0.0002 (3)	0.0074 (3)	0.0013 (3)
C9_2	0.0176 (4)	0.0153 (4)	0.0129 (4)	0.0008 (3)	0.0058 (3)	0.0016 (3)
C10_2	0.0174 (4)	0.0142 (4)	0.0114 (4)	0.0003 (3)	0.0051 (3)	0.0005 (3)
C11_2	0.0186 (4)	0.0137 (4)	0.0126 (4)	0.0000 (3)	0.0054 (3)	-0.0004 (3)
C12_2	0.0235 (5)	0.0217 (5)	0.0126 (4)	-0.0019 (4)	0.0059 (4)	-0.0006 (3)
N1_2	0.0200 (4)	0.0148 (4)	0.0125 (3)	0.0010 (3)	0.0059 (3)	-0.0009 (3)
O1_2	0.0313 (4)	0.0172 (3)	0.0137 (3)	0.0026 (3)	0.0050 (3)	0.0015 (3)
O2_2	0.0254 (3)	0.0176 (3)	0.0150 (3)	-0.0003 (3)	0.0076 (3)	-0.0039 (2)
O3_2	0.0219 (3)	0.0142 (3)	0.0126 (3)	0.0006 (2)	0.0065 (2)	-0.0008 (2)
O4_2	0.0256 (4)	0.0201 (3)	0.0136 (3)	0.0021 (3)	0.0065 (3)	0.0027 (2)
O5_2	0.0271 (4)	0.0164 (3)	0.0135 (3)	0.0007 (3)	0.0055 (3)	-0.0012 (2)

Geometric parameters (\AA , $^\circ$)

C1_1—C2_1	1.5098 (13)	C1_2—C2_2	1.5087 (13)
C1_1—C4_1	1.4719 (12)	C1_2—C4_2	1.4673 (12)
C1_1—O1_1	1.2132 (11)	C1_2—O1_2	1.2165 (11)
C2_1—C3_1	1.4764 (12)	C2_2—C3_2	1.4832 (12)
C2_1—O2_1	1.2147 (11)	C2_2—O2_2	1.2141 (11)
C3_1—C4_1	1.4130 (12)	C3_2—C4_2	1.4096 (12)
C3_1—N1_1	1.3329 (11)	C3_2—N1_2	1.3297 (11)
C4_1—O3_1	1.3106 (10)	C4_2—O3_2	1.3148 (10)
C5_1—H5A_1	1.077 (14)	C5_2—H5A_2	1.094 (14)
C5_1—H5B_1	1.073 (15)	C5_2—H5B_2	1.075 (14)
C5_1—H5C_1	1.078 (13)	C5_2—H5C_2	1.074 (14)
C5_1—O3_1	1.4551 (11)	C5_2—O3_2	1.4522 (11)
C6_1—C7_1	1.3972 (12)	C6_2—C7_2	1.3951 (12)
C6_1—C11_1	1.4061 (12)	C6_2—C11_2	1.4077 (12)
C6_1—N1_1	1.4133 (11)	C6_2—N1_2	1.4127 (11)
C7_1—H7_1	1.078 (13)	C7_2—H7_2	1.093 (14)
C7_1—C8_1	1.4041 (13)	C7_2—C8_2	1.4009 (13)
C8_1—H8_1	1.077 (14)	C8_2—H8_2	1.100 (15)
C8_1—C9_1	1.3787 (13)	C8_2—C9_2	1.3740 (13)
C9_1—C10_1	1.3881 (12)	C9_2—C10_2	1.3886 (12)
C9_1—O4_1	1.3657 (11)	C9_2—O4_2	1.3692 (11)
C10_1—C11_1	1.3753 (12)	C10_2—C11_2	1.3751 (12)
C10_1—O5_1	1.3641 (11)	C10_2—O5_2	1.3678 (11)
C11_1—H11_1	1.088 (13)	C11_2—H11_2	1.085 (13)
C12_1—H12A_1	1.089 (13)	C12_2—H12A_2	1.093 (14)
C12_1—H12B_1	1.073 (14)	C12_2—H12B_2	1.080 (14)
C12_1—O4_1	1.4294 (13)	C12_2—O4_2	1.4287 (12)
C12_1—O5_1	1.4411 (11)	C12_2—O5_2	1.4371 (11)
N1_1—H1_1	1.037 (15)	N1_2—H1_2	1.026 (15)
C4_1—C1_1—C2_1	87.06 (7)	C4_2—C1_2—C2_2	87.40 (7)
O1_1—C1_1—C2_1	135.62 (8)	O1_2—C1_2—C2_2	135.53 (8)
O1_1—C1_1—C4_1	137.29 (9)	O1_2—C1_2—C4_2	137.06 (9)

C3_1—C2_1—C1_1	89.14 (7)	C3_2—C2_2—C1_2	88.71 (7)
O2_1—C2_1—C1_1	135.95 (9)	O2_2—C2_2—C1_2	135.94 (8)
O2_1—C2_1—C3_1	134.91 (9)	O2_2—C2_2—C3_2	135.33 (9)
C4_1—C3_1—C2_1	90.57 (7)	C4_2—C3_2—C2_2	90.57 (7)
N1_1—C3_1—C2_1	128.14 (8)	N1_2—C3_2—C2_2	128.19 (8)
N1_1—C3_1—C4_1	141.27 (8)	N1_2—C3_2—C4_2	141.23 (8)
C3_1—C4_1—C1_1	93.16 (7)	C3_2—C4_2—C1_2	93.26 (7)
O3_1—C4_1—C1_1	134.24 (8)	O3_2—C4_2—C1_2	134.35 (8)
O3_1—C4_1—C3_1	132.60 (8)	O3_2—C4_2—C3_2	132.37 (8)
H5B_1—C5_1—H5A_1	111.7 (11)	H5B_2—C5_2—H5A_2	110.9 (10)
H5C_1—C5_1—H5A_1	109.7 (10)	H5C_2—C5_2—H5A_2	109.6 (10)
H5C_1—C5_1—H5B_1	110.2 (11)	H5C_2—C5_2—H5B_2	109.5 (10)
O3_1—C5_1—H5A_1	109.4 (7)	O3_2—C5_2—H5A_2	109.1 (7)
O3_1—C5_1—H5B_1	106.6 (8)	O3_2—C5_2—H5B_2	107.7 (7)
O3_1—C5_1—H5C_1	109.2 (7)	O3_2—C5_2—H5C_2	110.0 (7)
C11_1—C6_1—C7_1	121.04 (8)	C11_2—C6_2—C7_2	121.05 (8)
N1_1—C6_1—C7_1	117.83 (8)	N1_2—C6_2—C7_2	116.95 (8)
N1_1—C6_1—C11_1	121.13 (8)	N1_2—C6_2—C11_2	122.00 (8)
H7_1—C7_1—C6_1	118.5 (7)	H7_2—C7_2—C6_2	120.1 (7)
C8_1—C7_1—C6_1	121.20 (9)	C8_2—C7_2—C6_2	121.42 (9)
C8_1—C7_1—H7_1	120.2 (7)	C8_2—C7_2—H7_2	118.4 (7)
H8_1—C8_1—C7_1	121.1 (7)	H8_2—C8_2—C7_2	120.9 (8)
C9_1—C8_1—C7_1	117.20 (9)	C9_2—C8_2—C7_2	117.01 (8)
C9_1—C8_1—H8_1	121.7 (7)	C9_2—C8_2—H8_2	122.1 (8)
C10_1—C9_1—C8_1	121.10 (8)	C10_2—C9_2—C8_2	121.40 (8)
O4_1—C9_1—C8_1	129.10 (9)	O4_2—C9_2—C8_2	128.73 (8)
O4_1—C9_1—C10_1	109.80 (8)	O4_2—C9_2—C10_2	109.85 (8)
C11_1—C10_1—C9_1	123.02 (9)	C11_2—C10_2—C9_2	122.90 (8)
O5_1—C10_1—C9_1	109.97 (8)	O5_2—C10_2—C9_2	109.65 (7)
O5_1—C10_1—C11_1	127.00 (8)	O5_2—C10_2—C11_2	127.43 (8)
C10_1—C11_1—C6_1	116.38 (8)	C10_2—C11_2—C6_2	116.19 (8)
H11_1—C11_1—C6_1	123.9 (7)	H11_2—C11_2—C6_2	122.3 (7)
H11_1—C11_1—C10_1	119.7 (7)	H11_2—C11_2—C10_2	121.5 (7)
H12B_1—C12_1—H12A_1	113.8 (10)	H12B_2—C12_2—H12A_2	112.9 (10)
O4_1—C12_1—H12A_1	109.3 (7)	O4_2—C12_2—H12A_2	109.3 (7)
O4_1—C12_1—H12B_1	109.8 (7)	O4_2—C12_2—H12B_2	108.5 (8)
O5_1—C12_1—H12A_1	107.8 (7)	O5_2—C12_2—H12A_2	110.1 (7)
O5_1—C12_1—H12B_1	108.4 (7)	O5_2—C12_2—H12B_2	108.3 (8)
O5_1—C12_1—O4_1	107.63 (7)	O5_2—C12_2—O4_2	107.66 (7)
C6_1—N1_1—C3_1	128.52 (8)	C6_2—N1_2—C3_2	129.28 (8)
H1_1—N1_1—C3_1	116.2 (8)	H1_2—N1_2—C3_2	113.4 (8)
H1_1—N1_1—C6_1	115.0 (8)	H1_2—N1_2—C6_2	115.9 (8)
C5_1—O3_1—C4_1	116.12 (7)	C5_2—O3_2—C4_2	115.42 (7)
C12_1—O4_1—C9_1	106.25 (7)	C12_2—O4_2—C9_2	105.89 (7)
C12_1—O5_1—C10_1	105.83 (7)	C12_2—O5_2—C10_2	105.86 (7)
C1_1—C2_1—C3_1—C4_1	-2.16 (7)	C1_2—C2_2—C3_2—C4_2	1.59 (7)
C1_1—C2_1—C3_1—N1_1	176.34 (6)	C1_2—C2_2—C3_2—N1_2	-178.77 (6)

C1_1—C4_1—C3_1—C2_1	2.22 (7)	C1_2—C4_2—C3_2—C2_2	-1.64 (7)
C1_1—C4_1—C3_1—N1_1	-175.90 (7)	C1_2—C4_2—C3_2—N1_2	178.82 (7)
C1_1—C4_1—O3_1—C5_1	4.84 (13)	C1_2—C4_2—O3_2—C5_2	-8.27 (12)
C2_1—C3_1—C4_1—O3_1	-178.29 (6)	C2_2—C3_2—C4_2—O3_2	176.92 (6)
C2_1—C3_1—N1_1—C6_1	-178.45 (9)	C2_2—C3_2—N1_2—C6_2	-173.79 (9)
C3_1—C4_1—O3_1—C5_1	-174.45 (10)	C3_2—C4_2—O3_2—C5_2	173.75 (10)
C3_1—N1_1—C6_1—C7_1	-164.77 (10)	C3_2—N1_2—C6_2—C7_2	161.89 (10)
C3_1—N1_1—C6_1—C11_1	15.64 (11)	C3_2—N1_2—C6_2—C11_2	-18.46 (11)
C6_1—C7_1—C8_1—C9_1	-0.81 (11)	C6_2—C7_2—C8_2—C9_2	0.28 (11)
C6_1—C11_1—C10_1—C9_1	-1.65 (10)	C6_2—C11_2—C10_2—C9_2	0.66 (10)
C6_1—C11_1—C10_1—O5_1	179.13 (7)	C6_2—C11_2—C10_2—O5_2	-177.63 (7)
C7_1—C8_1—C9_1—C10_1	1.78 (11)	C7_2—C8_2—C9_2—C10_2	-1.11 (11)
C7_1—C8_1—C9_1—O4_1	-178.25 (8)	C7_2—C8_2—C9_2—O4_2	177.37 (8)
C8_1—C9_1—C10_1—C11_1	-0.56 (12)	C8_2—C9_2—C10_2—C11_2	0.64 (11)
C8_1—C9_1—C10_1—O5_1	178.78 (9)	C8_2—C9_2—C10_2—O5_2	179.20 (9)
C8_1—C9_1—O4_1—C12_1	176.58 (11)	C8_2—C9_2—O4_2—C12_2	174.65 (11)
C9_1—C10_1—O5_1—C12_1	5.25 (9)	C9_2—C10_2—O5_2—C12_2	5.97 (9)
C9_1—O4_1—C12_1—O5_1	6.60 (8)	C9_2—O4_2—C12_2—O5_2	10.30 (7)
C10_1—O5_1—C12_1—O4_1	-7.28 (7)	C10_2—O5_2—C12_2—O4_2	-10.03 (7)

Hydrogen-bond geometry (Å, °)

D—H···A	D—H	H···A	D···A	D—H···A
N1_1—H1_1···O2_2	1.037 (15)	1.864 (15)	2.8963 (10)	172.9 (12)
N1_2—H1_2···O2_1	1.026 (15)	1.901 (15)	2.8772 (10)	157.8 (12)

3-[(Benzo-1,3-dioxol-5-yl)amino]-4-methoxycyclobut-3-ene-1,2-dione (3-II)*Crystal data*

C ₁₂ H ₉ NO ₅	Z = 4
M _r = 247.20	F(000) = 512
Triclinic, P1	D _x = 1.579 Mg m ⁻³
a = 3.7001 (4) Å	Mo Kα radiation, λ = 0.71073 Å
b = 12.4583 (15) Å	Cell parameters from 6912 reflections
c = 22.846 (3) Å	θ = 2.4–24.9°
α = 89.550 (8)°	μ = 0.13 mm ⁻¹
β = 86.967 (6)°	T = 100 K
γ = 81.460 (6)°	Needle, colourless
V = 1040.0 (2) Å ³	0.12 × 0.05 × 0.03 mm

Data collection

Bruker D8 Venture	76269 measured reflections
diffractometer	5138 independent reflections
Radiation source: microfocus X-ray tube	3902 reflections with $I > 2\sigma(I)$
Detector resolution: 7.391 pixels mm ⁻¹	$R_{\text{int}} = 0.134$
φ- and ω-scans	$\theta_{\text{max}} = 28.4^\circ$, $\theta_{\text{min}} = 2.4^\circ$
Absorption correction: gaussian	$h = -4 \rightarrow 4$
(SADABS; Bruker, 2016)	$k = -16 \rightarrow 16$
$T_{\text{min}} = 0.991$, $T_{\text{max}} = 0.998$	$l = -30 \rightarrow 30$

Refinement

Refinement on F^2
 Least-squares matrix: full
 $R[F^2 > 2\sigma(F^2)] = 0.064$
 $wR(F^2) = 0.170$
 $S = 1.04$
 5138 reflections
 337 parameters
 1 restraint
 Primary atom site location: dual
 Secondary atom site location: difference Fourier map
 Hydrogen site location: mixed

H atoms treated by a mixture of independent and constrained refinement
 $w = 1/[\sigma^2(F_o^2) + (0.0992P)^2 + 0.138P]$
 where $P = (F_o^2 + 2F_c^2)/3$
 $(\Delta/\sigma)_{\text{max}} < 0.001$
 $\Delta\rho_{\text{max}} = 0.38 \text{ e } \text{\AA}^{-3}$
 $\Delta\rho_{\text{min}} = -0.35 \text{ e } \text{\AA}^{-3}$
 Extinction correction: SHELXL2019 (Sheldrick, 2015*b*),
 $F_c^* = kFc[1 + 0.001xFc^2\lambda^3/\sin(2\theta)]^{-1/4}$
 Extinction coefficient: 0.042 (6)

Special details

Geometry. All esds (except the esd in the dihedral angle between two l.s. planes) are estimated using the full covariance matrix. The cell esds are taken into account individually in the estimation of esds in distances, angles and torsion angles; correlations between esds in cell parameters are only used when they are defined by crystal symmetry. An approximate (isotropic) treatment of cell esds is used for estimating esds involving l.s. planes.

Refinement. Refined as a 2-component twin.

Fractional atomic coordinates and isotropic or equivalent isotropic displacement parameters (\AA^2)

	<i>x</i>	<i>y</i>	<i>z</i>	$U_{\text{iso}}^*/U_{\text{eq}}$
C1_1	0.2402 (10)	0.7866 (3)	0.51046 (13)	0.0255 (7)
C2_1	0.1226 (10)	0.6755 (3)	0.51094 (13)	0.0250 (7)
C3_1	0.2399 (10)	0.6649 (3)	0.44813 (13)	0.0247 (7)
C4_1	0.3445 (10)	0.7697 (3)	0.44802 (13)	0.0237 (7)
C5_1	0.5495 (10)	0.9354 (3)	0.42243 (14)	0.0268 (7)
H5A_1	0.695205	0.930734	0.457201	0.040*
H5B_1	0.313730	0.981055	0.431108	0.040*
H5C_1	0.681263	0.967252	0.389944	0.040*
C6_1	0.3797 (10)	0.5791 (3)	0.35222 (13)	0.0251 (7)
C7_1	0.5768 (10)	0.4828 (3)	0.33207 (14)	0.0285 (8)
H7_1	0.612141	0.421794	0.357437	0.034*
C8_1	0.7247 (10)	0.4745 (3)	0.27456 (14)	0.0285 (8)
H8_1	0.858046	0.408337	0.259804	0.034*
C9_1	0.6700 (10)	0.5655 (3)	0.24018 (13)	0.0257 (7)
C10_1	0.4620 (10)	0.6604 (3)	0.26002 (13)	0.0258 (7)
C11_1	0.3108 (10)	0.6714 (3)	0.31610 (13)	0.0255 (7)
H11_1	0.168412	0.736995	0.329787	0.031*
C12_1	0.6376 (11)	0.6866 (3)	0.16599 (14)	0.0324 (8)
H12A_1	0.465799	0.681057	0.134751	0.039*
H12B_1	0.829074	0.728670	0.150642	0.039*
N1_1	0.2392 (9)	0.5827 (2)	0.41202 (11)	0.0259 (6)
H1_1	0.187 (14)	0.517 (3)	0.430 (2)	0.055 (14)*
O1_1	0.2459 (8)	0.8580 (2)	0.54614 (10)	0.0321 (6)
O2_1	-0.0123 (7)	0.6176 (2)	0.54736 (10)	0.0289 (6)
O3_1	0.4870 (7)	0.82578 (19)	0.40592 (9)	0.0259 (5)
O4_1	0.7999 (8)	0.5808 (2)	0.18365 (10)	0.0328 (6)

O5_1	0.4462 (8)	0.7392 (2)	0.21652 (10)	0.0351 (6)
C1_2	-0.0234 (10)	0.2902 (3)	-0.01201 (13)	0.0251 (7)
C2_2	0.1966 (10)	0.1789 (3)	-0.01516 (13)	0.0252 (7)
C3_2	0.1312 (9)	0.1663 (3)	0.04828 (13)	0.0237 (7)
C4_2	-0.0716 (10)	0.2701 (3)	0.05150 (13)	0.0236 (7)
C5_2	-0.4349 (10)	0.4327 (3)	0.08122 (15)	0.0281 (7)
H5A_2	-0.582883	0.427038	0.047354	0.042*
H5B_2	-0.255440	0.481501	0.071770	0.042*
H5C_2	-0.594347	0.461496	0.114837	0.042*
C6_2	0.1661 (10)	0.0821 (3)	0.14662 (12)	0.0245 (7)
C7_2	0.0471 (10)	-0.0099 (3)	0.17147 (14)	0.0257 (7)
H7_2	0.004350	-0.067252	0.146838	0.031*
C8_2	-0.0108 (10)	-0.0188 (3)	0.23268 (14)	0.0286 (8)
H8_2	-0.094132	-0.080522	0.250434	0.034*
C9_2	0.0609 (10)	0.0671 (3)	0.26493 (13)	0.0239 (7)
C10_2	0.1883 (10)	0.1576 (3)	0.23942 (13)	0.0247 (7)
C11_2	0.2434 (9)	0.1692 (3)	0.18013 (13)	0.0241 (7)
H11_2	0.327330	0.231263	0.162966	0.029*
C12_2	0.1126 (11)	0.1850 (3)	0.33644 (13)	0.0286 (8)
H12A_2	0.290638	0.183380	0.367415	0.034*
H12B_2	-0.115970	0.232001	0.349835	0.034*
N1_2	0.2357 (9)	0.0846 (2)	0.08406 (11)	0.0261 (6)
H1_2	0.347 (12)	0.017 (3)	0.0690 (19)	0.043 (12)*
O1_2	-0.1202 (7)	0.3619 (2)	-0.04711 (10)	0.0308 (6)
O2_2	0.3643 (8)	0.1206 (2)	-0.05342 (10)	0.0311 (6)
O3_2	-0.2439 (7)	0.32517 (19)	0.09569 (9)	0.0274 (5)
O4_2	0.0395 (8)	0.07640 (19)	0.32501 (10)	0.0298 (6)
O5_2	0.2608 (7)	0.22682 (19)	0.28226 (9)	0.0271 (5)

Atomic displacement parameters (\AA^2)

	U^{11}	U^{22}	U^{33}	U^{12}	U^{13}	U^{23}
C1_1	0.0336 (19)	0.0267 (17)	0.0162 (14)	-0.0040 (14)	-0.0017 (13)	0.0011 (12)
C2_1	0.0349 (19)	0.0242 (16)	0.0156 (14)	-0.0020 (14)	-0.0061 (13)	0.0009 (12)
C3_1	0.0355 (19)	0.0230 (16)	0.0156 (14)	-0.0033 (14)	-0.0027 (12)	0.0004 (12)
C4_1	0.0292 (18)	0.0259 (17)	0.0174 (14)	-0.0078 (13)	-0.0030 (13)	-0.0018 (12)
C5_1	0.038 (2)	0.0245 (17)	0.0192 (15)	-0.0081 (14)	-0.0047 (13)	-0.0011 (12)
C6_1	0.0335 (19)	0.0289 (17)	0.0136 (13)	-0.0070 (14)	-0.0014 (12)	-0.0019 (12)
C7_1	0.040 (2)	0.0257 (17)	0.0204 (15)	-0.0062 (15)	-0.0047 (14)	0.0001 (12)
C8_1	0.041 (2)	0.0227 (17)	0.0211 (15)	-0.0025 (15)	-0.0046 (14)	-0.0023 (12)
C9_1	0.0336 (19)	0.0278 (17)	0.0158 (14)	-0.0039 (14)	-0.0017 (12)	-0.0065 (12)
C10_1	0.0333 (19)	0.0263 (16)	0.0192 (14)	-0.0078 (14)	-0.0030 (13)	-0.0019 (12)
C11_1	0.0352 (19)	0.0225 (16)	0.0196 (14)	-0.0058 (14)	-0.0049 (13)	-0.0019 (12)
C12_1	0.045 (2)	0.0362 (19)	0.0163 (15)	-0.0061 (17)	-0.0012 (14)	-0.0007 (14)
N1_1	0.0389 (17)	0.0239 (15)	0.0160 (12)	-0.0066 (13)	-0.0041 (11)	-0.0006 (11)
O1_1	0.0536 (17)	0.0276 (13)	0.0173 (11)	-0.0125 (11)	-0.0016 (10)	-0.0055 (9)
O2_1	0.0414 (15)	0.0283 (13)	0.0180 (11)	-0.0090 (11)	-0.0017 (10)	0.0005 (9)
O3_1	0.0408 (14)	0.0248 (12)	0.0137 (10)	-0.0109 (11)	-0.0005 (9)	-0.0011 (9)

O4_1	0.0489 (16)	0.0322 (13)	0.0157 (10)	-0.0008 (12)	-0.0034 (10)	-0.0024 (10)
O5_1	0.0567 (17)	0.0303 (13)	0.0160 (10)	0.0003 (12)	0.0005 (11)	-0.0014 (9)
C1_2	0.0332 (19)	0.0243 (17)	0.0178 (14)	-0.0030 (14)	-0.0056 (13)	-0.0014 (12)
C2_2	0.0342 (19)	0.0255 (17)	0.0162 (14)	-0.0050 (14)	-0.0032 (13)	-0.0024 (12)
C3_2	0.0309 (18)	0.0260 (16)	0.0152 (14)	-0.0065 (14)	-0.0030 (12)	-0.0035 (12)
C4_2	0.0333 (18)	0.0235 (16)	0.0144 (13)	-0.0055 (14)	0.0000 (12)	-0.0006 (12)
C5_2	0.035 (2)	0.0237 (17)	0.0246 (15)	-0.0016 (14)	-0.0037 (14)	-0.0017 (13)
C6_2	0.0345 (19)	0.0251 (16)	0.0131 (14)	-0.0009 (14)	-0.0035 (12)	0.0005 (12)
C7_2	0.036 (2)	0.0223 (15)	0.0188 (15)	-0.0018 (14)	-0.0063 (13)	-0.0021 (12)
C8_2	0.037 (2)	0.0250 (17)	0.0233 (16)	-0.0023 (14)	-0.0023 (14)	0.0010 (13)
C9_2	0.0316 (18)	0.0276 (17)	0.0111 (13)	-0.0002 (14)	0.0003 (12)	0.0020 (12)
C10_2	0.0329 (19)	0.0229 (15)	0.0181 (14)	-0.0029 (14)	-0.0030 (13)	-0.0023 (12)
C11_2	0.0305 (18)	0.0236 (16)	0.0181 (14)	-0.0040 (13)	0.0001 (12)	-0.0013 (12)
C12_2	0.041 (2)	0.0297 (18)	0.0156 (14)	-0.0067 (15)	0.0000 (14)	-0.0012 (13)
N1_2	0.0372 (17)	0.0239 (14)	0.0157 (12)	0.0009 (12)	-0.0038 (11)	-0.0023 (11)
O1_2	0.0426 (16)	0.0301 (14)	0.0181 (11)	-0.0003 (11)	-0.0016 (10)	0.0008 (9)
O2_2	0.0450 (16)	0.0301 (13)	0.0166 (11)	-0.0002 (11)	-0.0013 (10)	-0.0044 (9)
O3_2	0.0390 (14)	0.0267 (12)	0.0152 (10)	-0.0009 (10)	0.0007 (9)	-0.0059 (9)
O4_2	0.0493 (16)	0.0271 (13)	0.0138 (10)	-0.0090 (11)	-0.0001 (10)	0.0000 (9)
O5_2	0.0435 (15)	0.0263 (12)	0.0122 (10)	-0.0077 (10)	-0.0009 (9)	-0.0021 (8)

Geometric parameters (\AA , $^\circ$)

C1_1—O1_1	1.215 (4)	C1_2—C4_2	1.476 (4)
C1_1—C4_1	1.467 (4)	C1_2—C2_2	1.501 (5)
C1_1—C2_1	1.510 (5)	C2_2—O2_2	1.223 (4)
C2_1—O2_1	1.231 (4)	C2_2—C3_2	1.468 (4)
C2_1—C3_1	1.478 (4)	C2_2—C4_2	2.032 (5)
C3_1—N1_1	1.321 (4)	C3_2—N1_2	1.325 (4)
C3_1—C4_1	1.415 (5)	C3_2—C4_2	1.396 (5)
C4_1—O3_1	1.318 (4)	C4_2—O3_2	1.307 (4)
C5_1—O3_1	1.474 (4)	C5_2—O3_2	1.462 (4)
C5_1—H5A_1	0.9800	C5_2—H5A_2	0.9800
C5_1—H5B_1	0.9800	C5_2—H5B_2	0.9800
C5_1—H5C_1	0.9800	C5_2—H5C_2	0.9800
C6_1—C7_1	1.377 (5)	C6_2—C7_2	1.393 (5)
C6_1—C11_1	1.409 (5)	C6_2—C11_2	1.405 (4)
C6_1—N1_1	1.435 (4)	C6_2—N1_2	1.440 (4)
C7_1—C8_1	1.395 (5)	C7_2—C8_2	1.410 (5)
C7_1—H7_1	0.9500	C7_2—H7_2	0.9500
C8_1—C9_1	1.370 (5)	C8_2—C9_2	1.370 (5)
C8_1—H8_1	0.9500	C8_2—H8_2	0.9500
C9_1—O4_1	1.376 (4)	C9_2—O4_2	1.376 (3)
C9_1—C10_1	1.378 (5)	C9_2—C10_2	1.397 (5)
C10_1—C11_1	1.370 (4)	C10_2—C11_2	1.369 (4)
C10_1—O5_1	1.389 (4)	C10_2—O5_2	1.372 (4)
C11_1—H11_1	0.9500	C11_2—H11_2	0.9500
C12_1—O4_1	1.429 (5)	C12_2—O4_2	1.447 (4)

C12_1—O5_1	1.432 (4)	C12_2—O5_2	1.452 (4)
C12_1—H12A_1	0.9900	C12_2—H12A_2	0.9900
C12_1—H12B_1	0.9900	C12_2—H12B_2	0.9900
N1_1—H1_1	0.94 (3)	N1_2—H1_2	0.94 (3)
C1_2—O1_2	1.222 (4)		
O1_1—C1_1—C4_1	136.3 (3)	O2_2—C2_2—C3_2	133.7 (3)
O1_1—C1_1—C2_1	136.0 (3)	O2_2—C2_2—C1_2	136.4 (3)
C4_1—C1_1—C2_1	87.7 (2)	C3_2—C2_2—C1_2	89.9 (3)
O2_1—C2_1—C3_1	135.0 (3)	O2_2—C2_2—C4_2	177.1 (3)
O2_1—C2_1—C1_1	136.3 (3)	C3_2—C2_2—C4_2	43.41 (18)
C3_1—C2_1—C1_1	88.6 (3)	C1_2—C2_2—C4_2	46.46 (18)
N1_1—C3_1—C4_1	139.5 (3)	N1_2—C3_2—C4_2	138.3 (3)
N1_1—C3_1—C2_1	129.6 (3)	N1_2—C3_2—C2_2	131.3 (3)
C4_1—C3_1—C2_1	90.9 (3)	C4_2—C3_2—C2_2	90.3 (3)
O3_1—C4_1—C3_1	131.3 (3)	O3_2—C4_2—C3_2	131.5 (3)
O3_1—C4_1—C1_1	135.8 (3)	O3_2—C4_2—C1_2	134.8 (3)
C3_1—C4_1—C1_1	92.8 (3)	C3_2—C4_2—C1_2	93.7 (3)
O3_1—C5_1—H5A_1	109.5	O3_2—C4_2—C2_2	177.6 (3)
O3_1—C5_1—H5B_1	109.5	C3_2—C4_2—C2_2	46.25 (19)
H5A_1—C5_1—H5B_1	109.5	C1_2—C4_2—C2_2	47.47 (18)
O3_1—C5_1—H5C_1	109.5	O3_2—C5_2—H5A_2	109.5
H5A_1—C5_1—H5C_1	109.5	O3_2—C5_2—H5B_2	109.5
H5B_1—C5_1—H5C_1	109.5	H5A_2—C5_2—H5B_2	109.5
C7_1—C6_1—C11_1	122.3 (3)	O3_2—C5_2—H5C_2	109.5
C7_1—C6_1—N1_1	117.5 (3)	H5A_2—C5_2—H5C_2	109.5
C11_1—C6_1—N1_1	120.2 (3)	H5B_2—C5_2—H5C_2	109.5
C6_1—C7_1—C8_1	120.3 (3)	C7_2—C6_2—C11_2	123.0 (3)
C6_1—C7_1—H7_1	119.9	C7_2—C6_2—N1_2	118.4 (3)
C8_1—C7_1—H7_1	119.9	C11_2—C6_2—N1_2	118.5 (3)
C9_1—C8_1—C7_1	117.4 (3)	C6_2—C7_2—C8_2	120.9 (3)
C9_1—C8_1—H8_1	121.3	C6_2—C7_2—H7_2	119.6
C7_1—C8_1—H8_1	121.3	C8_2—C7_2—H7_2	119.6
C8_1—C9_1—O4_1	129.1 (3)	C9_2—C8_2—C7_2	115.7 (3)
C8_1—C9_1—C10_1	122.0 (3)	C9_2—C8_2—H8_2	122.1
O4_1—C9_1—C10_1	108.9 (3)	C7_2—C8_2—H8_2	122.1
C11_1—C10_1—C9_1	122.2 (3)	C8_2—C9_2—O4_2	127.0 (3)
C11_1—C10_1—O5_1	127.4 (3)	C8_2—C9_2—C10_2	122.7 (3)
C9_1—C10_1—O5_1	110.4 (3)	O4_2—C9_2—C10_2	110.2 (3)
C10_1—C11_1—C6_1	115.8 (3)	C11_2—C10_2—O5_2	127.1 (3)
C10_1—C11_1—H11_1	122.1	C11_2—C10_2—C9_2	122.9 (3)
C6_1—C11_1—H11_1	122.1	O5_2—C10_2—C9_2	110.0 (3)
O4_1—C12_1—O5_1	107.5 (3)	C10_2—C11_2—C6_2	114.8 (3)
O4_1—C12_1—H12A_1	110.2	C10_2—C11_2—H11_2	122.6
O5_1—C12_1—H12A_1	110.2	C6_2—C11_2—H11_2	122.6
O4_1—C12_1—H12B_1	110.2	O4_2—C12_2—O5_2	107.7 (2)
O5_1—C12_1—H12B_1	110.2	O4_2—C12_2—H12A_2	110.2
H12A_1—C12_1—H12B_1	108.5	O5_2—C12_2—H12A_2	110.2

C3_1—N1_1—C6_1	124.8 (3)	O4_2—C12_2—H12B_2	110.2
C3_1—N1_1—H1_1	116 (3)	O5_2—C12_2—H12B_2	110.2
C6_1—N1_1—H1_1	118 (3)	H12A_2—C12_2—H12B_2	108.5
C4_1—O3_1—C5_1	115.5 (2)	C3_2—N1_2—C6_2	126.9 (3)
C9_1—O4_1—C12_1	107.1 (2)	C3_2—N1_2—H1_2	121 (3)
C10_1—O5_1—C12_1	105.6 (3)	C6_2—N1_2—H1_2	112 (3)
O1_2—C1_2—C4_2	138.1 (3)	C4_2—O3_2—C5_2	115.3 (3)
O1_2—C1_2—C2_2	135.8 (3)	C9_2—O4_2—C12_2	105.0 (2)
C4_2—C1_2—C2_2	86.1 (2)	C10_2—O5_2—C12_2	105.1 (3)
O1_1—C1_1—C2_1—O2_1	0.7 (8)	O1_2—C1_2—C2_2—C3_2	-178.2 (4)
C4_1—C1_1—C2_1—O2_1	-179.4 (4)	C4_2—C1_2—C2_2—C3_2	0.4 (3)
O1_1—C1_1—C2_1—C3_1	-179.2 (4)	O1_2—C1_2—C2_2—C4_2	-178.6 (6)
C4_1—C1_1—C2_1—C3_1	0.7 (3)	O2_2—C2_2—C3_2—N1_2	-0.7 (7)
O2_1—C2_1—C3_1—N1_1	-2.1 (7)	C1_2—C2_2—C3_2—N1_2	179.5 (4)
C1_1—C2_1—C3_1—N1_1	177.8 (4)	C4_2—C2_2—C3_2—N1_2	179.8 (5)
O2_1—C2_1—C3_1—C4_1	179.3 (4)	O2_2—C2_2—C3_2—C4_2	179.4 (4)
C1_1—C2_1—C3_1—C4_1	-0.7 (3)	C1_2—C2_2—C3_2—C4_2	-0.4 (3)
N1_1—C3_1—C4_1—O3_1	1.5 (8)	N1_2—C3_2—C4_2—O3_2	-0.8 (7)
C2_1—C3_1—C4_1—O3_1	179.8 (4)	C2_2—C3_2—C4_2—O3_2	179.0 (4)
N1_1—C3_1—C4_1—C1_1	-177.6 (5)	N1_2—C3_2—C4_2—C1_2	-179.4 (4)
C2_1—C3_1—C4_1—C1_1	0.8 (3)	C2_2—C3_2—C4_2—C1_2	0.4 (3)
O1_1—C1_1—C4_1—O3_1	0.2 (8)	N1_2—C3_2—C4_2—C2_2	-179.8 (6)
C2_1—C1_1—C4_1—O3_1	-179.7 (4)	O1_2—C1_2—C4_2—O3_2	-0.4 (8)
O1_1—C1_1—C4_1—C3_1	179.2 (4)	C2_2—C1_2—C4_2—O3_2	-178.9 (4)
C2_1—C1_1—C4_1—C3_1	-0.8 (3)	O1_2—C1_2—C4_2—C3_2	178.1 (4)
C11_1—C6_1—C7_1—C8_1	1.7 (5)	C2_2—C1_2—C4_2—C3_2	-0.4 (3)
N1_1—C6_1—C7_1—C8_1	-179.2 (3)	O1_2—C1_2—C4_2—C2_2	178.5 (6)
C6_1—C7_1—C8_1—C9_1	1.0 (5)	C11_2—C6_2—C7_2—C8_2	1.5 (5)
C7_1—C8_1—C9_1—O4_1	176.4 (4)	N1_2—C6_2—C7_2—C8_2	177.3 (3)
C7_1—C8_1—C9_1—C10_1	-3.3 (5)	C6_2—C7_2—C8_2—C9_2	-0.6 (5)
C8_1—C9_1—C10_1—C11_1	3.0 (6)	C7_2—C8_2—C9_2—O4_2	-177.4 (3)
O4_1—C9_1—C10_1—C11_1	-176.7 (3)	C7_2—C8_2—C9_2—C10_2	-0.9 (5)
C8_1—C9_1—C10_1—O5_1	-179.2 (3)	C8_2—C9_2—C10_2—C11_2	1.7 (6)
O4_1—C9_1—C10_1—O5_1	1.0 (4)	O4_2—C9_2—C10_2—C11_2	178.7 (3)
C9_1—C10_1—C11_1—C6_1	-0.3 (5)	C8_2—C9_2—C10_2—O5_2	-175.7 (3)
O5_1—C10_1—C11_1—C6_1	-177.7 (3)	O4_2—C9_2—C10_2—O5_2	1.4 (4)
C7_1—C6_1—C11_1—C10_1	-2.0 (5)	O5_2—C10_2—C11_2—C6_2	176.1 (3)
N1_1—C6_1—C11_1—C10_1	178.9 (3)	C9_2—C10_2—C11_2—C6_2	-0.8 (5)
C4_1—C3_1—N1_1—C6_1	1.5 (7)	C7_2—C6_2—C11_2—C10_2	-0.8 (5)
C2_1—C3_1—N1_1—C6_1	-176.3 (3)	N1_2—C6_2—C11_2—C10_2	-176.6 (3)
C7_1—C6_1—N1_1—C3_1	138.8 (4)	C4_2—C3_2—N1_2—C6_2	-2.5 (7)
C11_1—C6_1—N1_1—C3_1	-42.0 (5)	C2_2—C3_2—N1_2—C6_2	177.7 (3)
C3_1—C4_1—O3_1—C5_1	178.2 (4)	C7_2—C6_2—N1_2—C3_2	134.7 (4)
C1_1—C4_1—O3_1—C5_1	-3.1 (6)	C11_2—C6_2—N1_2—C3_2	-49.3 (5)
C8_1—C9_1—O4_1—C12_1	174.8 (4)	C3_2—C4_2—O3_2—C5_2	-178.8 (3)
C10_1—C9_1—O4_1—C12_1	-5.4 (4)	C1_2—C4_2—O3_2—C5_2	-0.7 (6)
O5_1—C12_1—O4_1—C9_1	7.7 (4)	C8_2—C9_2—O4_2—C12_2	-175.5 (4)

C11_1—C10_1—O5_1—C12_1	−178.6 (4)	C10_2—C9_2—O4_2—C12_2	7.6 (4)
C9_1—C10_1—O5_1—C12_1	3.8 (4)	O5_2—C12_2—O4_2—C9_2	−13.4 (3)
O4_1—C12_1—O5_1—C10_1	−7.0 (4)	C11_2—C10_2—O5_2—C12_2	173.1 (4)
O1_2—C1_2—C2_2—O2_2	2.0 (8)	C9_2—C10_2—O5_2—C12_2	−9.7 (4)
C4_2—C1_2—C2_2—O2_2	−179.4 (5)	O4_2—C12_2—O5_2—C10_2	14.3 (3)

Hydrogen-bond geometry (Å, °)

D—H···A	D—H	H···A	D···A	D—H···A
N1_1—H1_1···O2_1 ⁱ	0.94 (3)	1.95 (4)	2.880 (4)	168 (4)
N1_2—H1_2···O2_2 ⁱⁱ	0.94 (3)	1.91 (3)	2.831 (4)	167 (4)

Symmetry codes: (i) $-x, -y+1, -z+1$; (ii) $-x+1, -y, -z$.